Freeze-frame imaging of synaptic activity using SynTagMA

Alberto Perez-Alvarez[1*], Brenna C. Fearey[1*], Christian Schulze[1], Ryan J. O'Toole[2], Benjamien Moeyaert[3], Manuel A. Mohr[3], Ignacio Arganda-Carreras[4,5,6], Wei Yang[7], J. Simon Wiegert[7], Eric R. Schreiter[3], Christine E. Gee[1], Michael B. Hoppa[2], Thomas G. Oertner[1§]

[1] Institute for Synaptic Physiology, University Medical Center Hamburg-Eppendorf, Hamburg, Germany

[2] Department of Biological Sciences, Dartmouth College, Hanover, NH, USA

[3] HHMI, Janelia Farm Research Campus, VA, USA

[4]Ikerbasque, Basque Foundation for Science, Bilbao, Spain

[5]Dept. of Computer Science and Artificial Intelligence, Basque Country University, San Sebastian, Spain

[6]Donostia International Physics Center (DIPC), San Sebastian, Spain

[7]Research Group Synaptic Wiring and Information Processing, University Medical Center Hamburg-Eppendorf, Hamburg, Germany

* These authors contributed equally to the study

[§] Corresponding author. E-mail: thomas.oertner@zmnh.uni-hamburg.de

ABSTRACT

Information within the brain travels from neuron to neuron across synapses. At any given moment, only a few synapses within billions will be active and are thought to transmit key information about the environment, a behavior being executed or memory being recalled. Here we present SynTagMA, which marks active synapses within a ~2 s time window. Upon violet illumination, the genetically expressed tag converts from green to red fluorescence if bound to calcium. Targeted to presynaptic terminals, preSynTagMA allows discrimination between active and silent axons. Targeted to excitatory postsynapses, postSynTagMA creates a snapshot of synapses active just before photoconversion. To analyze large datasets, we developed an analysis program that automatically identifies and tracks the fluorescence of thousands of individual synapses in tissue. Together, these tools provide a high throughput method for repeatedly mapping active synapses *in vitro* and *in vivo*.

MAIN

The physical changes underlying learning and memory likely involve alterations in the strength and/or number of synaptic connections. On the network level, neuroscience faces an extreme 'needle in the haystack' problem: it is thought to be impossible, in practice, to localize and track the few synapses that carry a specific memory trace. If it were feasible to acquire a complete map of synaptic activity before and after learning, a comparison of the two activity maps would reveal the subset of connections that changed their properties, i.e. the synaptic engram. Two-photon laser-scanning microscopy enables monitoring the activity of many neurons and even single synapses in highly light-scattering brain tissue [1]. However, the tradeoff between spatial and temporal resolution makes it impossible to simultaneously monitor the tiny and fleeting fluorescence transients of Ca^{2+} or voltage indicators from the thousands of synapses of even a single pyramidal neuron. Most functional imaging experiments are therefore limited to cell bodies, i.e. low spatial resolution[2], or are restricted to monitoring the simultaneous activity of a few synapses within a single focal plane[3]. Multi-beam scanning designs have been proposed, but due to scattering of emitted photons, they do not produce sharp images at depth[4,5]. The need to choose between temporal and spatial resolution limits the information we can extract from the brain with optical methods.

A strategy to overcome this limit is to rapidly 'freeze' activity in a defined time window and read it out at high resolution later. The Ca^{2+}-modulated photoactivatable ratiometric integrator CaMPARI undergoes an irreversible chromophore change from green to red when the Ca^{2+} bound form is irradiated with violet light[6,7]. CaMPARI has been successfully applied to map the activity of thousands of neurons in zebrafish, *Drosophila*, and in mouse[6,8–10].

As CaMPARI was designed to diffuse freely within the cytoplasm, it does not preserve subcellular details of Ca^{2+} signaling. By anchoring CaMPARI to either pre- or postsynaptic compartments, we developed tools that mark active synapses in short time windows defined by violet illumination. Three steps were necessary to create a **Syn**aptic **Tag** for **M**apping **A**ctivity (SynTagMA): 1) We improved the brightness and conversion efficiency of CaMPARI[7]; 2) We targeted CaMPARI2 (F391W_L398V) to either presynaptic boutons by fusing it to synaptophysin (preSynTagMA) or to the postsynaptic density by fusing it to an intrabody against PSD95[11] (postSynTagMA); 3) We developed an analysis workflow that corrects for chromatic aberration, tissue displacement (warping) and automatically finds regions of interest (i.e. postsynapses or boutons) to quantify green and red fluorescence. Bouton-localized preSynTagMA allowed us to distinguish active and inactive axons. Spine-localized postSynTagMA allowed us to map the extent of action potential back-propagation into the large apical dendritic tree of hippocampal pyramidal cells. Following repeated sparse activation of Schaffer collateral

axons, postSynTagMA marks a small subset of synapses on CA1 pyramidal cells as highly active. PostSynTagMA is not only useful to analyze the organization of inputs on pyramidal cells, but works equally well to map shaft synapses on aspiny interneurons.

RESULTS

Creating and characterizing a presynaptic marker of activity

To visualize activated presynaptic boutons, we fused the Ca^{2+}-modulated photoactivatable ratiometric integrator CaMPARI[6] to the vesicular protein synaptophysin (sypCaMPARI). In cultured hippocampal neurons, sypCaMPARI showed a punctate expression pattern along the axon, indicating successful targeting to vesicle clusters in presynaptic boutons (**Fig. 1a, f**). CaMPARI fluorescence dims when Ca^{2+} binds[6]. Similarly, sypCaMPARI fluorescence decreased after stimulating neurons to evoke trains of action potentials (APs), saturating at 50 APs (**Fig. 1b-d**). Indeed, the signal-to-noise ratio was sufficient for detecting single APs in single boutons when 30 sweeps were averaged, suggesting a high sensitivity of localized sypCaMPARI for Ca^{2+} influx (**Fig. 1c**). The Ca^{2+}-bound form of CaMPARI is irreversibly photoconverted from a green to a red fluorescent state by violet light irradiation[6]. Repeatedly pairing electrical field stimulation with violet light flashes increased the red-to-green fluorescence ratio (R/G) of sypCaMPARI boutons in a stepwise fashion (**Fig. 1e and f**). Blocking action potential generation with tetrodotoxin (TTX) strongly reduced photoconversion, indicating that spike-induced Ca^{2+} influx through high-threshold voltage-activated Ca^{2+} channels was necessary for efficient conversion. Similar to the dimming response, the amount of sypCaMPARI photoconversion depended on the number of APs (**Fig. 1g**), suggesting that the R/G ratio can be interpreted as a lasting and quantitative record of axonal activity rather than just a binary signal.

Ca^{2+}-dependent dimming of sypCaMPARI peaked about 1 s after stimulation and returned to baseline after 3-10 s, and the Ca^{2+}-bound form is known to be most sensitive to violet light. To determine the photoconversion time window, multiple delays were tested in single experiments using a digital mirror device (**Fig. 2a**). Photoconversion of sypCaMPARI was not efficient when violet light pulses (100 ms duration) were coincident with stimulation onset (**Fig. 2b, c**). Rather, maximal photoconversion occurred when violet light was applied 2 s after stimulation. The photoconversion window of sypCaMPARI extended to at least 10 s after stimulation, outlasting the dimming response to 5 APs (**Fig. 2b, c, Fig. 1b**). Some photoconversion also occurred in the absence of stimulation or in the presence of TTX (**Fig. 1e, g, 2b, c, Supplementary Fig. 1**). The long time window and activity-independent photoconversion are both undesirable traits that limit the utility of sypCaMPARI.

Parallel efforts to improve CaMPARI resulted in CaMPARI2, which contains a number of point mutations improving brightness, increasing kinetics, reducing activity-independent photoconversion and lowering the Ca^{2+} affinity[7]. We selected the variant CaMPARI2 (F391W_L398V) (K_d Ca^{2+} = 174 nM, k_{on} 66 s^{-1}, k_{off} 0.37 s^{-1}, photoconversion rate in slices 0.22 s^{-1} with Ca^{2+}, 0.0021 s^{-1} without Ca^{2+})[7] and fused it to synaptophysin to create preSynTagMA. The temporal precision and dynamic range of preSynTagMA were both enhanced. PreSynTagMA showed no photoconversion in the absence of stimulation and the photoconversion time window was shortened to 0.2 – 2 s post-stimulation, corresponding to the faster dimming in response to 50 APs (**Fig. 2d, e, Supplementary Fig. 2**). Using preSynTagMA, we could readily distinguish active from inactive axons in the presence of bicuculline (**Supplementary Fig. 2**). Blocking action potentials (TTX) completely prevented SynTagMA photoconversion. Two hours after photoconversion, the R/G ratio was still 68% of the peak value, indicating preSynTagMA marks activated synapses for at least several hours. To quantify preSynTagMA localization in tissue, we co-expressed preSynTagMA together with cytosolic mCerulean in hippocampal slice cultures. Using two-photon excitation at 840 nm (mCerulean) and 980 nm (preSynTagMA green) we again observed green fluorescent puncta at axonal boutons (**Fig. 2g**). Compared to mCerulean, preSynTagMA was 3-fold enriched in boutons vs. axonal shafts (**Fig. 2h**).

Targeting SynTagMA to excitatory postsynapses

We chose to target SynTagMA to the postsynaptic protein PSD95, which has a higher retention time than most postsynaptic density proteins[12]. We decided against making a PSD95-CaMPARI fusion protein as overexpression of PSD95 is known to induce dramatic changes in function, size, and connectivity of dendritic spines [13]. Instead, we fused CaMPARI2 (F391W_L398V) (after deleting the nuclear export sequence) to a genetically encoded intrabody against PSD95 (PSD95.FingR), which provides high specificity without measurable effects on synaptic function[11]. However, green fluorescence was not limited to dendritic spines, where most excitatory synapses are located, but was detected throughout the dendrites of CA1 pyramidal neurons (**Fig. 3a**). We reasoned that the lack of spine enrichment was due to a large fraction of unbound cytoplasmic protein. An elegant method to reduce cytoplasmic fluorescence is to fuse a zinc finger (ZF) and the transcription repressor KRAB(A) to the targeted protein and include a ZF binding sequence near the promoter[14,15]. As long as all proteins are sequestered by binding of the intrabody to PSD95, transcription proceeds. When, however, unbound SynTagMA enters the nucleus, the ZF domain binds to the plasmid, shutting down further transcription. We added these additional regulatory elements to the original construct and co-expressed it with mCerulean. Punctate green fluorescence was now observed predominantly in spines. The ratio of spine-to-dendrite green fluorescence was about 4 times higher than mCerulean spine-to-dendrite ratios, suggesting CaMPARI2 was now localized to

postsynapses (**Fig. 3b**). Serendipitously, we discovered that the upstream ZF binding sequence was dispensable for autoregulation (**Fig. 3c, d**). Nuclei were also fluorescent, indicating sequestration of non-synaptic protein to the nucleus. We named this simpler construct postSynTagMA and characterized it further.

Using back-propagating action potentials to characterize postSynTagMA

We evoked backpropagating action potentials (bAPs) by brief somatic current injections to raise intracellular Ca^{2+}, and applied violet light pulses (500 ms) with a 1 s delay to characterize postSynTagMA photoconversion. In the absence of stimulation (0 bAPs), violet illumination did not change the R/G ratio ($R_1/G_1 = R_0/G_0$). Pairing violet light with bAP trains (15 repeats) lead to increased R_1/G_1 ratios (**Fig 4a**). To determine the best metric for quantifying SynTagMA photoconversion, we plotted several against the initial green fluorescence, which indicates synapse size (**Fig. 4b, Supplementary Fig. 3**). Considering only the change in red fluorescence ($\Delta R = R_1 - R_0$), the apparent photoconversion positively correlated with synapse size (0 bAPs: $r_s = 0.11$ $p = 0.03$, 3 bAPs: $r_s = 0.23$ $p < 0.0001$, 50 bAPs: $r_s = 0.34$ $p < 0.0001$) and only large synapses in the 3 bAP and 50 bAP groups could be separated from the non-converted (0 bAP) synapses. The R_1/G_1 ratio, albeit showing better separation than ΔR, negatively correlated with size showing higher values and a higher chance to classify small synapses as photoconverted (**Fig. 4b**). When strong photoconversion occurs, small synapses with few indicator molecules may lose all green signal, which is problematic when one wishes to divide by this measure. Evidence of this is seen in the extremely high values (i.e. 20 - 200) for R_1/G_1, especially in small to medium-sized synapses (**Fig. 4a**). As photoconversion both increases red and decreases green fluorescence, we reasoned that using all channels before and after conversion would provide an optimal metric and avoid dividing by values close to 0. Indeed, $\Delta R/(G_0 + G_1)$ shows no correlation with PSD size (0 bAP: $r_s = -0.07$ $p = 0.164$, 3bAPs: $r_s = -0.03$ $p = 0.583$, 50 bAPs: $r_s = 0.004$ $p = 0.876$). Using this measure, we detected a significant increase in photoconversion after 15 x 50 bAPs and even after 15 x 3 bAPs (**Fig. 4c, d**; Kruskal-Wallis test $p < 0.0001$, Dunn's test for multiple comparison 0 bAP vs. 3 bAPs: mean rank difference = -342; 0 bAP vs. 50 bAPs: mean rank difference = -1133).

Analysis workflow for automatic synapse detection and quantification of SynTagMA

While the efficient targeting of SynTagMA allows simultaneous interrogation of a large population of synapses, it also presents an analysis challenge. To place regions of interest (ROIs) on individual synapses (**Figs. 1 and 2**), simple spot detection algorithms (e.g. Imaris, ImageJ) can be used, but matching of objects across several time points is not straightforward. When the number of synapses reaches into the thousands, a manually curated approach is not feasible. We therefore describe an image analysis workflow to tackle this problem (**Fig. 5**). Images acquired using two-photon excitation at different wavelengths must first undergo correction for laser alignment and chromatic aberration (**Fig. 5a**). As synapses in tissue are quite motile even on short time

scales[16,17], a non-rigid 3D transformation, termed 'unwarping', was applied to re-align and preserve synapse identity across time points. To achieve the highest quality transformation, images were first deconvolved and then underwent 'unwarping' (**Fig. 5b-c**). Synapses were then detected on transformed datasets using the Spot feature of Imaris (Bitplane AG) (**Fig. 5d**). Although each of these steps can be performed using a combination of freely and commercially available software packages (see **Material & Methods**), it is a time-consuming process that generates several gigabytes of data in intermediate steps. We therefore developed SynapseLocator (available at GitHub), a Matlab-based program with a user interface to streamline these aforementioned steps using freely available ancillary software tools (Fiji[18], DeconvolutionLab2[19], FeatureJ, elastix[20]). A machine-learning approach[21] was implemented to generate synapse templates (boutons or postsynaptic sites) that were used to automatically detect and extract fluorescence values by SynapseLocator. Transformed images and fluorescence values from identified synapses (ROIs) were saved for statistical analysis and imported into ImageJ or Imaris for 3D visualization (**Fig. 5d**). A specific difficulty for automated analysis is the presence of spot-like red autofluorescence at 1040 nm excitation. Synapses with elevated R_0/G_0 values at baseline were considered too close to autofluorescent objects and were automatically excluded from further analysis. Automation of the synapse identification process greatly reduced the analysis time (from days for ~500 hand-curated ROIs at several time points to minutes for ~4000 automatically detected ROIs from the same dataset, using a personal computer). Manual and automated analysis produced comparable results (**Supplementary Fig. 4**).

Back-propagating action potentials increase Ca^{2+} in a subset of dendritic spines

For a given number of bAPs, the amount of photoconversion was quite variable between individual spines (**Fig. 4a**), likely reflecting Ca^{2+} transients of different amplitude and duration. We also observed that whereas synapses close to the soma were strongly photoconverted, conversion decreased with distance (length constant λ = 105 µm; R^2 = 0.914), suggesting that bAPs do not increase [Ca^{2+}] in distal branches of the apical dendrite (**Fig. 5e, Supplementary Video 1**). Two control experiments were performed to corroborate this finding. PSD95 turns over in individual synapses with a time constant of 10 – 100 minutes[12,22]. As multiple stacks were required to image along the apical tree, we reversed the order of image acquisition, starting at the distal tuft. Again there was less photoconversion at distal synapses, verifying that decreased photoconversion in the distal tuft was not an artifact due to postSynTagMA turnover during acquisition (**Supplementary Fig. 5**). A further concern was that tuft synapses were outside the illumination field of the 40x objective, through which the violet light was applied. We therefore centered illumination over the distal tuft synapses during photoconversion and again observed very little photoconversion of distal tuft synapses. As the proximal synapses were now outside the field of

illumination, they were also not photoconverted (**Supplementary Fig. 5**). Thus, we mapped the extent of bAP-induced Ca^{2+}elevations across the dendritic tree using postSynTagMA.

Using postSynTagMA to map synaptic activity

We next wanted to drive spike trains in postSynTagMA-expressing CA1 neurons via synaptic activation. To adjust the stimulation intensity, we simultaneously recorded the membrane potential of a neighboring (non-transfected) neuron. PostSynTagMA-labelled synapses were strongly photoconverted during supra-threshold high frequency stimulation of Schaffer collateral axons (**Fig. 6a**). We then observed that R/G returned to baseline with a time constant of 56 min, in sharp contrast to the much slower turnover of preSynTagMA (**Fig. 6a**, **Supplementary Fig. 2**) and of photoconverted soluble CaMPARI (several days)[7]. This turnover limits the post-photoconversion acquisition time to about 30 minutes and is consistent with the turnover of synaptic PSD95[23]. On the other hand, rapid turnover enables multiple rounds of photoconversion, i.e. activated synapses can be remapped in a relatively short time span. Indeed, we were able to convert (median $\Delta R/(G_0 + G_1)$ = 1.26) and, 18 hours later, reconvert (median $\Delta R/(G_0 + G_1)$ = 1.25) a group of SynTagMA labeled spines, suggesting that multiple activity maps are feasible with postSynTagMA (**Fig. 6b**). However, as the postsynaptic neuron was spiking in these experiments, we could not distinguish spines that received direct synaptic input from spines that were passively flooded with Ca^{2+} (**Fig. 6c**).

We next tested whether subthreshold synaptic stimulation would sufficiently raise Ca^{2+} to photoconvert and mark active synapses with postSynTagMA. Violet light (100 ms) was applied 1 s after evoking sub-threshold synaptic responses (15-25 mV or -500 to -1000 pA), which assuming unitary responses of 0.9 mV or -18 pA[24] would mean 20-50 active synapses. In a 65 x 65 x 78 μm^3 volume containing a proximal region of the apical dendritic tree, we detected and analyzed 1500 postSynTagMA labeled synapses (**Fig. 6d, Supplementary Video 2**). Fourteen spines showed values above 3 σ ($\Delta R/(G_0 + G_1)$ = 0.97) and were therefore classified as active (**Fig. 6d**). This number is consistent with our expectations considering that we imaged approximately 10% of the entire dendritic tree[25,26].

To have an independent marker of synaptic activation, we stimulated presynaptic CA3 neurons expressing channelrhodopsin2 ET/TC (ChR2) and synaptophysin-mCerulean by blue light pulses[27]. Photoconverted spines on CA1 neurons adjacent to cyan fluorescent boutons were observed, suggesting that these synapses were directly innervated and activated by a ChR2 expressing presynaptic CA3 neuron (**Fig. 6e, Supplementary Video 3**).

PostSynTagMA maps active interneurons *in vivo*

In addition to the spine synapses in CA1 pyramidal neurons, postSynTagMA tags excitatory synapses on interneurons, showing puncta in dendrites and nuclear fluorescence in pyramidal layer interneurons in slice cultures (**Supplementary Fig. 6**). The same punctate dendritic and nuclear fluorescence was observed in *stratum oriens* interneurons in vivo (**Fig. 6e**). We implanted a cranial window above the dorsal hippocampus and imaged postSynTagMA-expressing interneurons in anesthetized mice. Time-lapse imaging of postSynTagMA revealed spontaneous dimming, indicating nuclear Ca^{2+} transients in some interneurons (**Supplementary Fig. 7**). Violet light photoconverted postSynTagMA in the nuclei of presumably active interneurons and not in neighboring interneurons (**Supplementary Fig. 8**). At the synaptic level, application of violet light pulses (3 s, 20 repeats) at low power (0.42 mW mm^{-2}) revealed dendrites with different amounts of photoconversion (**Fig. 6e**).

DISCUSSION

We have successfully created and characterized SynTagMA and demonstrated its usefulness for mapping active synapses either when targeted to presynaptic terminals by fusing it to the vesicle protein synaptophysin (preSynTagMA) or by targeting it to the postsynaptic scaffold of excitatory synapses (postSynTagMA). We have also demonstrated that it can be combined with a third fluorescent protein, here mCerulean, which is necessary to assign postSynTagMA puncta to particular dendrites or neurons. Both of the targeting strategies we used have been demonstrated to successfully label synapses with fluorescent proteins, without noticeably changing synaptic function[15,28]. PreSynTagMA should prove useful for identifying active axons in tissue and may also prove useful for distinguishing high from low release probability boutons based on the graded photoconversion. PostSynTagMA should likewise facilitate identification and mapping of active synapses, but on the postsynaptic side. Antibodies specific to the photoconverted red form will also enable further ultrastructural analysis of the marked synapses[7]. Identifying active synapses is a long-standing quest in neuroscience and several approaches have been put forward. Ca^{2+} precipitation in active spines was used to create an electron-dense label that can be detected by electron microscopy[29]. As this method requires tissue fixation, it does not allow monitoring changes in synaptic activity over time. Expressing the two halves of split-GFP on the extracellular surface of pre- and postsynaptic neurons (mGRASP) labels contact points between the neurons as green fluorescent puncta[30]. Refined transsynaptic labeling methods with multiple colors have led to remarkable insights about network connectivity[31,32]. Whereas mGRASP and eGRASP report anatomical connections, SynTagMA photoconversion is Ca^{2+}-dependent and therefore sensitive to synaptic activity. Several genetic strategies exist for labeling active neurons but they all operate on timescales much longer than the 2 s time window for SynTagMA[33]. One of the many interesting applications of postSynTagMA will be to create exhaustive input maps of individual neurons at

single synapse resolution. The question of whether inputs carrying similar information segregate to branches of the dendritic tree is currently being investigated using spine-by-spine Ca^{2+} imaging[3,34,35]. By freezing the activity status of all spines during a particular labelling protocol, SynTagMA may simplify such experiments by reading out fluorescence ratios in thousands of spines in a single high-resolution stack. Importantly, postSynTagMA maps can be repeated, opening the possibility to study the functional dynamics of excitatory connections rather than just morphology and turnover of dendritic spines.

In addition to input mapping, we envision several other applications for SynTagMA. For instance, it will be interesting to use SynTagMA to investigate the sources of synaptic Ca^{2+} transients. In addition to Ca^{2+} influx though voltage- or ligand-gated channels, Ca^{2+} can be released from intracellular stores in both presynaptic[36] and postsynaptic compartments[37–39]. Another application, used in this study is to investigate bAP-induced Ca^{2+} throughout a neuron. Ca^{2+} -dependent photoconversion was greatest in a subpopulation of spines relatively close to the soma (length constant = 105 µm) while distal synapses are predominately spared. This finding corroborates earlier findings and postSynTagMA may facilitate future studies designed to investigate the contribution of various ion channels and cell-specific differences in bAP propogation[40–42]. In addition to this distance-dependence, we observed that even close to the soma, conversion of spines was not very uniform and the same was true for boutons. Understanding the sources of this heterogeneity, and whether these correspond to particular classes of synapses may lead to important insights into network function.

A further unexpected application arises from the associated nuclear localization of postSynTagMA. As nuclear postSynTagMA also photoconverts on synaptically-activated or spiking neurons, this nuclear signal can be used to visualize the location of active neurons (e.g. Supplementary Figs. 7, 8). As the cytoplasm is almost free of label, automatic segmentation is very easy. Whereas pan-neuronal CaMPARI has been used to show regions of the nervous system active during behaviors in transparent organisms, the active cells cannot easily be identified as all processes are labelled as well[6–8]. We postulate that postSynTagMA would facilitate identification of the active neurons.

The sensitivity of SynTagMA to trains of bAPs is interesting, but will also interfere with SynTagMA-based input mapping if the postsynaptic neuron fires APs during strong (supra-threshold) synaptic activation. For input-mapping experiments, it is therefore advisable to repeat weak, subthreshold stimuli several times (15-50x), each time paired with a (delayed) pulse of violet light. Co-expression of an inhibitory tool that prevents spiking of the postSynTagMA neurons during imaging[43,44], would allow input mapping during strong excitatory episodes. In addition to synapses on mushroom-shaped spines, SynTagMA provides access to synapses on structures that are difficult to probe with Ca^{2+} dyes or diffusible GECIs, such as stubby spines or shaft synapses on pyramidal cells or

aspiny interneurons[45]. Thus, postSynTagMA may open the possibility to study the long-term dynamics of interneuron excitation, a key homeostatic mechanism that involves Ca^{2+}-induced-Ca^{2+} release from intracellular stores[46].

There are some caveats to working with SynTagMA. Before/during imaging, it is important to photoswitch with low intensity violet light into the bright state[6,7]. The quite rapid turnover of postSynTagMA means that after photoconversion images should be collected within about 30 minutes. SynTagMA analysis is further complicated by endogenous red fluorescence at 1040 nm excitation, which can be mistaken for photoconverted SynTagMA. For this reason, we found acquisition of a pre-photoconversion stack essential for reliable analysis: Synaptic ROIs (detected in the green channel) that already show elevated red fluorescence *before* stimulation (large R_0/G_0) can be classified as 'contaminated' and excluded from further analysis (see **Fig. 6a, f** for example red "spots" in both pre- and post-photoconversion images). If for experimental reasons only a single time point can be acquired, we recommend excluding objects that have high red fluorescence in the voxels surrounding green puncta. In our experiments we used two lasers to almost simultaneously collect green and red SynTagMA fluorescence by alternating plane by plane. We speculate that the very short time between collecting the red and green channels greatly helps to correct for chromatic aberrations and to unwarp and re-align the puncta at different time points. Also, when the two channels are not almost simultaneously collected, any Ca^{2+}-dependent dimming might occur on one and not the other channel. Particularly when imaging in vivo, the time required to re-tune a single laser to the different excitation wavelengths might make analysis of individual synapses impossible.

SynTagMA is amenable for viral delivery using recombinant AAVs. For *in vivo* experiments, it is impossible to assign synaptic puncta to individual neurons unless the dendritic (or axonal) trees do not overlap and there is an additional cytosolic fluorescent protein expressed in the same neurons (i.e. mCerulean or other cyan fluorescent protein). Using a promoter-based strategy, we demonstrate strong and sparse expression and photoconversion of postSynTagMA in hippocampal interneurons *in vivo* (**Fig. 6**). For sparse expression in pyramidal cells, dual-AAV labeling systems could be employed[47].

REFERENCES

1. Svoboda, K., Denk, W., Kleinfeld, D. & Tank, D. W. In vivo dendritic calcium dynamics in neocortical pyramidal neurons. *Nature* **385,** 161–165 (1997).
2. Grewe, B. F., Langer, D., Kasper, H., Kampa, B. M. & Helmchen, F. High-speed in vivo calcium imaging reveals neuronal network activity with near-millisecond precision. *Nature methods* **7,** 399–405 (2010).
3. Iacaruso, M. F., Gasler, I. T. & Hofer, S. B. Synaptic organization of visual space in primary visual cortex. *Nature* **547,** 449–452 (2017).

4. Andresen, V. *et al.* High-Resolution Intravital Microscopy. *PLoS ONE* **7,** e50915 (2012).
5. Bewersdorf, J., Pick, R. & Hell, S. W. Multifocal multiphoton microscopy. *Optics Letters* **23,** 655 (1998).
6. Fosque, B. F. *et al.* Labeling of active neural circuits in vivo with designed calcium integrators. *Science* **347,** 755–760 (2015).
7. Moeyaert, B. *et al.* Improved methods for marking active neuron populations. *Nature communications* **9,** 4440 (2018).
8. Patel, A. & Cox, D. Behavioral and Functional Assays for Investigating Mechanisms of Noxious Cold Detection and Multimodal Sensory Processing in Drosophila Larvae. *BIO-PROTOCOL* **7,** (2017).
9. Bohra, A. A., Kallman, B. R., Reichert, H. & VijayRaghavan, K. Identification of a Single Pair of Interneurons for Bitter Taste Processing in the Drosophila Brain. *Current Biology* **28,** 847–858.e3 (2018).
10. Zolnik, T. A. *et al.* All-optical functional synaptic connectivity mapping in acute brain slices using the calcium integrator CaMPARI. *The Journal of Physiology* **595,** 1465–1477 (2017).
11. Gross, G. G. *et al.* Recombinant probes for visualizing endogenous synaptic proteins in living neurons. *Neuron* **78,** 971–85 (2013).
12. Sturgill, J. F., Steiner, P., Czervionke, B. L. & Sabatini, B. L. Distinct domains within PSD-95 mediate synaptic incorporation, stabilization, and activity-dependent trafficking. *The Journal of neuroscience : the official journal of the Society for Neuroscience* **29,** 12845–54 (2009).
13. Nikonenko, I. *et al.* PSD-95 promotes synaptogenesis and multiinnervated spine formation through nitric oxide signaling. *J Cell Biol* **183,** 1115–1127 (2008).
14. Margolin, J. F. *et al.* Krüppel-associated boxes are potent transcriptional repression domains. *Proceedings of the National Academy of Sciences of the United States of America* **91,** 4509–13 (1994).
15. Gross, G. G. *et al.* Recombinant probes for visualizing endogenous synaptic proteins in living neurons. *Neuron* **78,** 971–85 (2013).
16. Bonhoeffer, T. & Yuste, R. Spine motility. Phenomenology, mechanisms, and function. *Neuron* **35,** 1019–27 (2002).
17. Fischer, M., Kaech, S., Knutti, D. & Matus, A. Rapid actin-based plasticity in dendritic spines. *Neuron* **20,** 847–54 (1998).
18. Schindelin, J. *et al.* Fiji: an open-source platform for biological-image analysis. *Nature Methods* **9,** 676–682 (2012).
19. Sage, D. *et al.* DeconvolutionLab2: An open-source software for deconvolution microscopy. *Methods* **115,** 28–41 (2017).
20. Klein, S., Staring, M., Murphy, K., Viergever, M. A. & Pluim, J. elastix: A Toolbox for Intensity-Based Medical Image Registration. *IEEE Transactions on Medical Imaging* **29,** 196–205 (2010).
21. Arganda-Carreras, I. *et al.* Trainable Weka Segmentation: a machine learning tool for microscopy pixel classification. *Bioinformatics (Oxford, England)* **33,** 2424–2426 (2017).
22. Gray, N. W., Weimer, R. M., Bureau, I. & Svoboda, K. Rapid redistribution of synaptic PSD-95 in the neocortex in vivo. *PLoS biology* **4,** e370 (2006).
23. Gray, N. W., Weimer, R. M., Bureau, I. & Svoboda, K. Rapid Redistribution of Synaptic PSD-95 in the Neocortex In Vivo. *PLoS Biology* **4,** e370 (2006).
24. Debanne, D., Guerineau, N. C., Gahwiler, B. H. & Thompson, S. M. Physiology and pharmacology of unitary synaptic connections between pairs of cells in areas CA3 and CA1 of rat hippocampal slice cultures. *Journal of Neurophysiology* **73,** 1282–1294 (1995).
25. Bannister, N. J. & Larkman, A. U. Dendritic morphology of CA1 pyramidal neurones from the rat hippocampus: II. Spine distributions. *The Journal of Comparative Neurology* **360,** 161–171 (1995).
26. Megías, M., Emri, Z., Freund, T. F. & Gulyás, A. I. Total number and distribution of inhibitory and excitatory synapses on hippocampal CA1 pyramidal cells. *Neuroscience* **102,** 527–40 (2001).
27. Berndt, A. *et al.* High-efficiency channelrhodopsins for fast neuronal stimulation at low light levels. *Proceedings of the National Academy of Sciences of the United States of America* **108,** 7595–600 (2011).

28. Li, Z. & Murthy, V. N. Visualizing Postendocytic Traffic of Synaptic Vesicles at Hippocampal Synapses. *Neuron* **31,** 593–605 (2001).
29. Toni, N., Buchs, P. A., Nikonenko, I., Bron, C. R. & Muller, D. LTP promotes formation of multiple spine synapses between a single axon terminal and a dendrite. *Nature* **402,** 421–425 (1999).
30. Feinberg, E. H. *et al.* GFP Reconstitution Across Synaptic Partners (GRASP) defines cell contacts and synapses in living nervous systems. *Neuron* **57,** 353–363 (2008).
31. Choi, J. H. *et al.* Interregional synaptic maps among engram cells underlie memory formation. *Science* **360,** (2018).
32. Macpherson, L. J. *et al.* Dynamic labelling of neural connections in multiple colours by trans-synaptic fluorescence complementation. *Nature Communications* **6,** 10024 (2015).
33. DeNardo, L. & Luo, L. Genetic strategies to access activated neurons. *Current Opinion in Neurobiology* **45,** 121–129 (2017).
34. Scholl, B., Wilson, D. E. & Fitzpatrick, D. Local Order within Global Disorder: Synaptic Architecture of Visual Space. *Neuron* **96,** 1127–1138.e4 (2017).
35. Chen, X., Leischner, U., Rochefort, N. L., Nelken, I. & Konnerth, A. Functional mapping of single spines in cortical neurons in vivo. *Nature* **475,** 501–505 (2011).
36. de Juan-Sanz, J. *et al.* Axonal Endoplasmic Reticulum Ca2+Content Controls Release Probability in CNS Nerve Terminals. *Neuron* **93,** 867–881.e6 (2017).
37. Sabatini, B. L., Oertner, T. G. & Svoboda, K. The life cycle of Ca(2+) ions in dendritic spines. *Neuron* **33,** 439–452 (2002).
38. Holbro, N., Grunditz, A. & Oertner, T. G. Differential distribution of endoplasmic reticulum controls metabotropic signaling and plasticity at hippocampal synapses. *Proceedings of the National Academy of Sciences of the United States of America* **106,** 15055–60 (2009).
39. Emptage, N., Bliss, T. V & Fine, A. Single synaptic events evoke NMDA receptor-mediated release of calcium from internal stores in hippocampal dendritic spines. *Neuron* **22,** 115–24 (1999).
40. Spruston, N., Schiller, Y., Stuart, G. & Sakmann, B. Activity-dependent action potential invasion and calcium influx into hippocampal CA1 dendrites. *Science (New York, N.Y.)* **268,** 297–300 (1995).
41. Yasuda, R., Sabatini, B. L. & Svoboda, K. Plasticity of calcium channels in dendritic spines. *Nature neuroscience* **6,** 948–55 (2003).
42. Golding, N. L., Kath, W. L. & Spruston, N. Dichotomy of action-potential backpropagation in CA1 pyramidal neuron dendrites. *Journal of neurophysiology* **86,** 2998–3010 (2001).
43. Wiegert, J. S., Mahn, M., Prigge, M., Printz, Y. & Yizhar, O. Silencing Neurons: Tools, Applications, and Experimental Constraints. *Neuron* **95,** 504–529 (2017).
44. Beck, S. *et al.* Synthetic Light-Activated Ion Channels for Optogenetic Activation and Inhibition. *Frontiers in neuroscience* **12,** 643 (2018).
45. Soler-Llavina, G. J. & Sabatini, B. L. Synapse-specific plasticity and compartmentalized signaling in cerebellar stellate cells. *Nat Neurosci* **9,** 798–806 (2006).
46. Topolnik, L. & Camiré, O. Non-linear calcium signalling and synaptic plasticity in interneurons. *Current Opinion in Neurobiology* **54,** 98–103 (2019).
47. Lin, R. *et al.* Cell-type-specific and projection-specific brain-wide reconstruction of single neurons. *Nature Methods* **15,** 1033–1036 (2018).

FIGURES

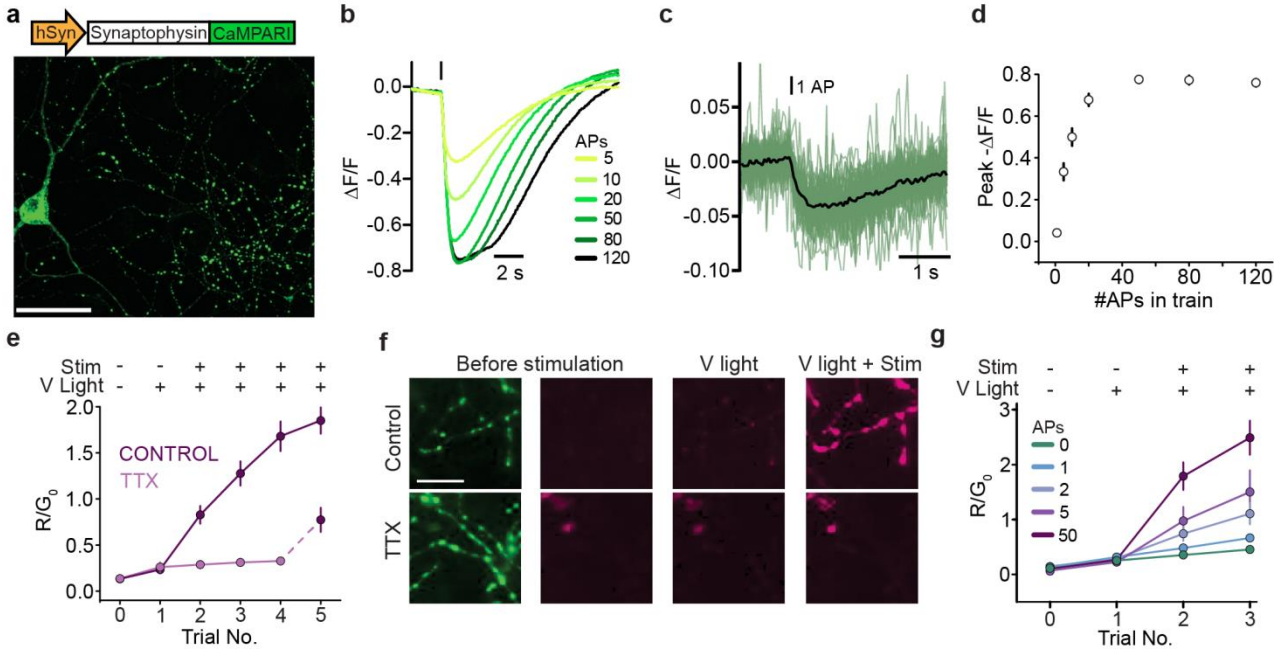

Figure 1 | Synaptophysin-fused CaMPARI marks active presynaptic terminals. (a) Representative image of cultured rat hippocampal neurons expressing sypCaMPARI showing punctate labeling in axonal boutons. Scale bar 50 µm. **(b)** Average fluorescence response of sypCaMPARI boutons (green channel emission) to varying numbers of action potentials (APs) evoked at 50 Hz (n = 6 neurons). **(c)** Trial-averaged responses to 30 single APs (green, n = 57 boutons). Black line is the average, representative of n = 3 neurons. **(d)** Plot of the maximum ΔF/F versus number of APs from the experiments in b) and c) (n = 6 cells, 317 synapses). **(e)** Plot of initial red to green ratio of boutons expressing sypCaMPARI (R_0/G_0, V light -, Stim -), after photoconverting violet light alone (405 nm, 20 flashes x 1 s, 0.1 Hz, 10.8 mW cm^{-2}, V light +, Stim -) and after simultaneous stimulation with trains of 50 APs at 50 Hz (V light +, Stim +, repeated 4 times). The experiment was performed in the absence or presence of 3 µM tetrodotoxin to block action potentials (control: n = 8 cells; TTX: n = 7 cells). Note that after washing out TTX, the R/G_0 ratio (V light + Stim +, trial 5) increased to the same extent as the first instance in control neurons (trial 2). **(f)** Representative red (magenta, Trial 0, Trial 1, Trial 3) and green (green, Trial 0) images of boutons from the experiment in e). The scale bar 20 µm applies to all panels in f. **(g)** The amount of photoconversion (R/G_0) in a similar experiment as e) but varying the number of APs in a 50 Hz train (V light 405 nm, 20 flashes x 1 s, 0.1 Hz, 54.1 mW cm^{-2}, Stim 20 bursts at 50 Hz). Data are mean ± SE (0 AP: n = 4 cells, 1 AP: n = 4, 2 APs: n = 5, 5 APs n = 5, 50 APs n = 7). 50 AP fold increase was statistically different from all other stimulation conditions using a one-way ANOVA with Tukey's post-hoc comparison ($p < 0.05$).

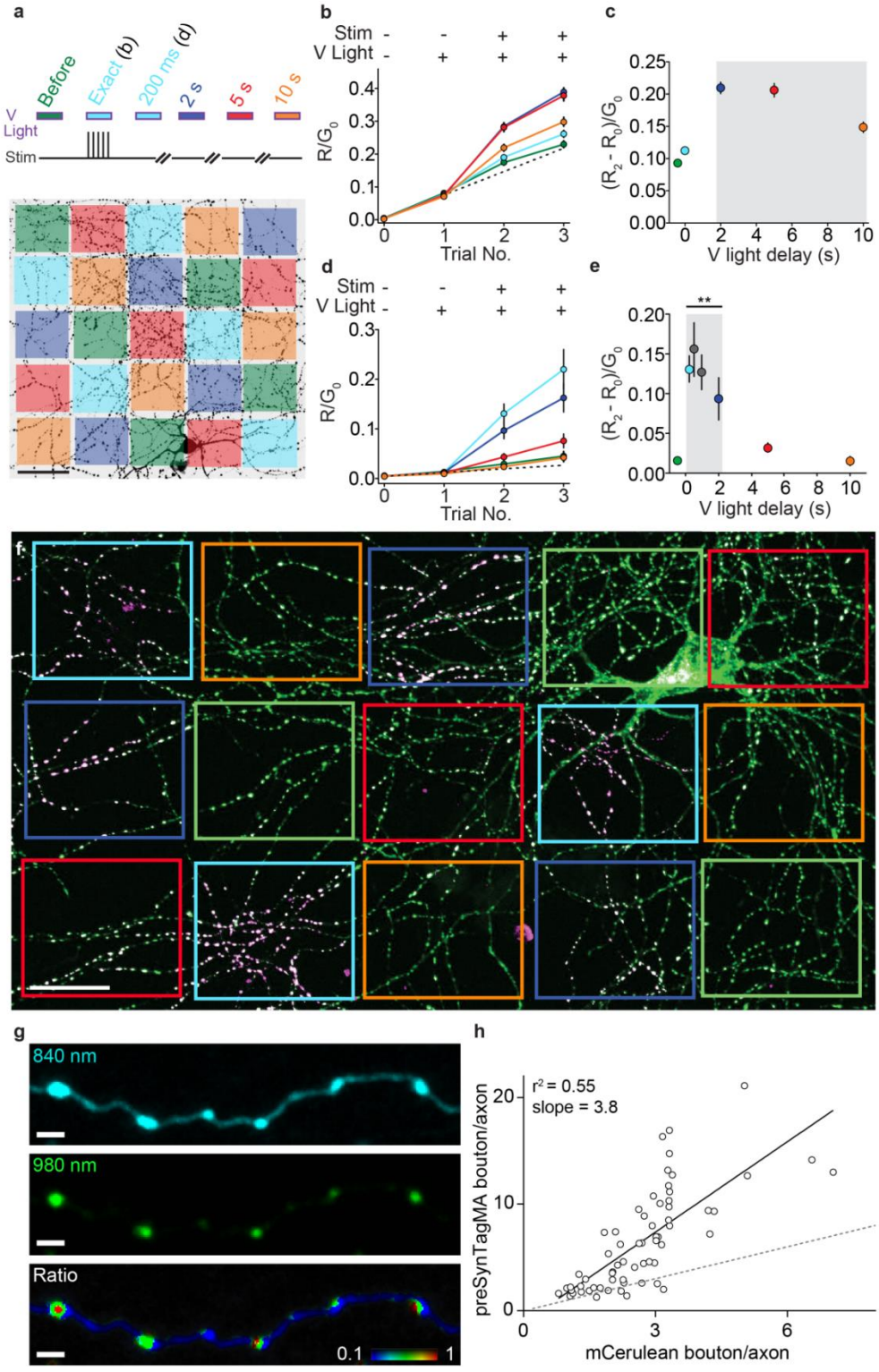

Figure 2 | Improved resolution of presynaptic SynTagMA. (a) Experimental design: Initial red (R_0) and green (G_0) fluorescent images were acquired of cultured rat hippocampal neurons. A computer-controlled spatial light modulator was used to apply timed photoconverting violet light (405 nm, 50 mW cm^{-2}) alone or at different time intervals relative to 5 APs @ 50 Hz in a grid pattern over the axonal arbor (repeated 5x, 30s intervals). After each

trial, new images were acquired and red fluorescence intensity ($R_{Trial\ No.}$) compared to the G_0. Note that both 'exact' & '200 ms' timing are cyan. sypCaMPARI experiments used 'exact' and preSynTagMA used '200 ms' timing in the cyan quadrant. **(b)** Ratio of red to green fluorescence (R/G_0) from sypCaMPARI boutons illuminated with various delays alone (Stim -, V light +, Trial 1) or together with APs (Stim +, V light +, Trial 2, 3). Lines have the same color code as panel a), n = 6 cells **(c)** Activity-dependent photoconversion ($\Delta R/G_0$) versus delay from start of stimulation to violet light from experiments in b). The grey box indicates the long time window (up to 10 s after activity) for efficient photoconversion of sypCaMPARI. **(d)** Neurons expressing preSynTagMA (synaptophysin-CaMPARI2 (F391W, L398V)) were stimulated as in a-c. Note the greatly reduced increase in R/G_0 with violet light alone. n = 6 cells **(e)** Activity-dependent photoconversion ($\Delta R/ G_0$) versus delay of preSynTagMA expressing neurons. The grey box indicates the much shorter time window (200 ms to 2 s after activity) for efficient photoconversion of SynTagMA. n = 12 cells total, 12 pre, 12 200 ms, 6 500 ms, 6 1 s, 12 2 s, 6 5 s, 6 10 s. **(f)** Cropped example of cultured rat hippocampal neurons expressing preSynTagMA after trial 3. Boxes indicate regions where photoconversion light was applied with different delays (color code as in panel a). **(g)** Two-photon images of axonal boutons in CA1 *stratum radiatum* originating from CA3 neurons expressing preSynTagMA and mCerulean as cytosolic filler (hippocampal slice cultures). Upper panel shows mCerulean fluorescence (excited at 840 nm), middle panel is preSynTagMA fluorescence (excited at 980 nm), lower panel is the ratio image. **(h)** The ratio of preSynTagMA bouton to axonal shaft fluorescence vs the ratio of mCerulean bouton to axon fluorescence for n = 64 boutons. Solid line is the linear fit to the data points, dashed line (slope = 1) indicates the theoretical 'no bouton enrichment' fit. Data in b-e) are presented as mean ± SE. Statistics were performed using Kruskal-Wallis ANOVA followed by Dunn's multiple comparison ** $p < 0.01$ vs pre. Scale bars: a) 50 µm, b) 25 µm, and g) 2 µm.

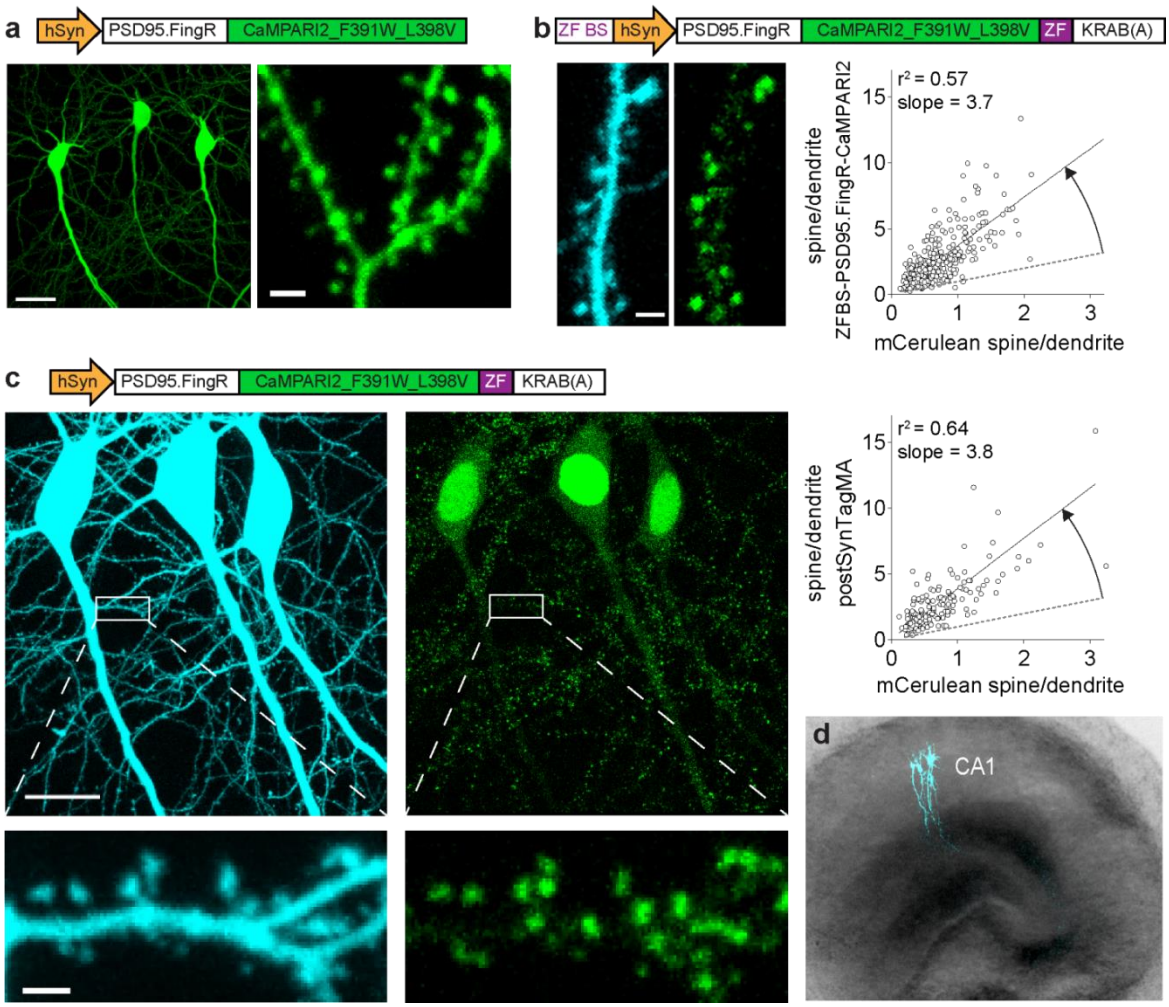

Figure 3 | Postsynaptic targeting of SynTagMA using a PSD95 intrabody.

(**a**) Two photon maximum intensity projection (excitation 980 nm) from CA1 neurons expressing a fusion protein of PSD95 fibronectin intrabody (PSD95.FingR) and CaMPARI2_F391W_L398V (without NES or epitope tags). Scale bars 20 µm, 2 µm respectively. (**b**) Two photon maximum intensity projections from a CA1 neuron expressing PSD95.FingR-CaMPARI2 with a zinc finger binding sequence (ZF BS) added upstream of the promoter and a zinc finger (ZF) fused to a transcriptional repressor domain (KRAB(A)) and mCerulean (excitation 840 nm). Plotted is the spine to dendrite green fluorescence ratio vs the cyan spine to dendrite ratio (1 slice, 3 neurons, 367 spines). Scale bar 2 µm. (**c**) Postsynaptically targeted SynTagMA (postSynTagMA). As in b) with the ZF-KRAB(A) but no upstream ZF-BS. Note that postSynTagMA is still enriched in spines and the nucleus, leaving the cytoplasm almost free of SynTagMA (2 slices, 3 neurons, 179 spines). Scale bars: upper 20 µm, lower 2 µm. **(d)** Overlayed bright field and epifluorescence images of three postSynTagMA/mCerulean expressing CA1 pyramidal cells. In all constructs, the CaMPARI2 sequence lacked the NES and epitope tags (see Material & Methods).

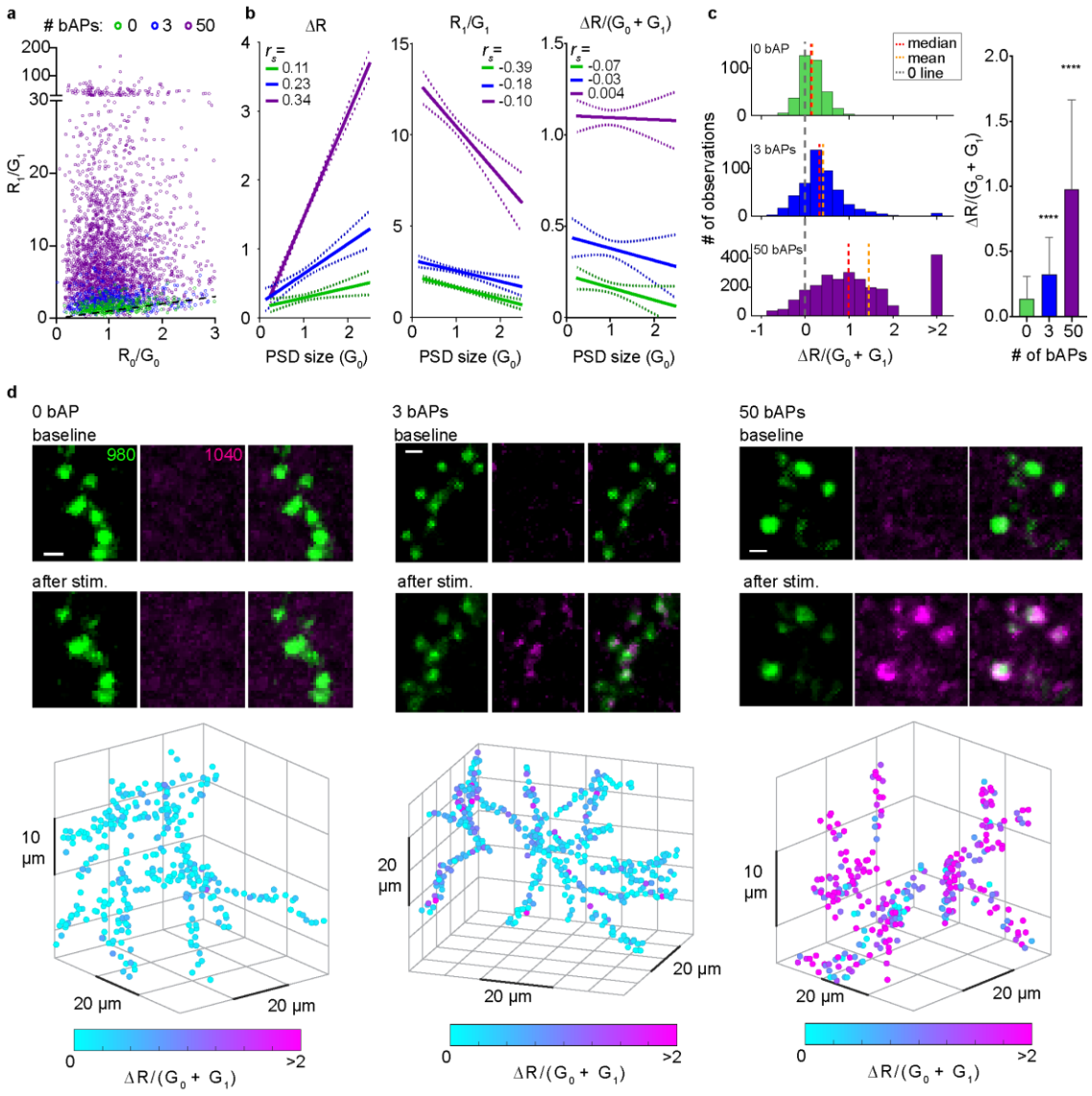

Figure 4 | PostSynTagMA photoconversion with back-propagating action potentials (bAPs).

Two-photon image stacks of postSynTagMA expressing CA1 pyramidal neurons (excitation 980 nm and 1040 nm) were taken before and after 15 pairings of trains of bAPs (100 Hz) with photoconverting violet light (395 nm, 16 mW mm^{-2}, 500 ms duration, 1 s delay). Synaptic transmission was blocked. **(a)** R/G ratios of individual synapses before (R_0/G_0) vs after (R_1/G_1) photoconversion. Note the variability in photoconversion within conditions. Dotted black line is the unity line. **(b)** Three different metrics vs PSD size (Magenta: 50 bAPs. Blue: 3 bAPs. Green: 0 bAP; linear regression lines with 95% confidence intervals). Note that for strong stimulation, the conversion factor metric $\Delta R/(G_0+G_1)$ does not depend on PSD size. r_s is Spearman's rho. **(c)** Distributions of photoconversion ($\Delta R/(G_0+G_1)$ for each condition (0bAP: median = 0.139 mean = 0.164; 3bAPs: median = 0.327 mean = 0.406; 50bAPs: median = 0.984 mean = 1.452) and $\Delta R/(G_0+G_1)$ vs the number of bAPs (data are median and interquartile range; ****$p < 0.0001$, Kruskal-Wallis vs. 0 bAP). N = 1 cell, 356 synapses (0 bAP), n = 1 cell, 472 synapses (3bAPs), n = 3 cells, 2587 synapses (50bAPs) **(d)** Example green, red and merged images of

SynTagMA labelled spines photoconverted with 0, 3 or 50 bAPs. Below the color-coded photoconversion factor of individual spines vs their 3D-positions in the dendritic arbor are plotted. Spines with values 2 and above are all magenta color. Scale bars 1 µm.

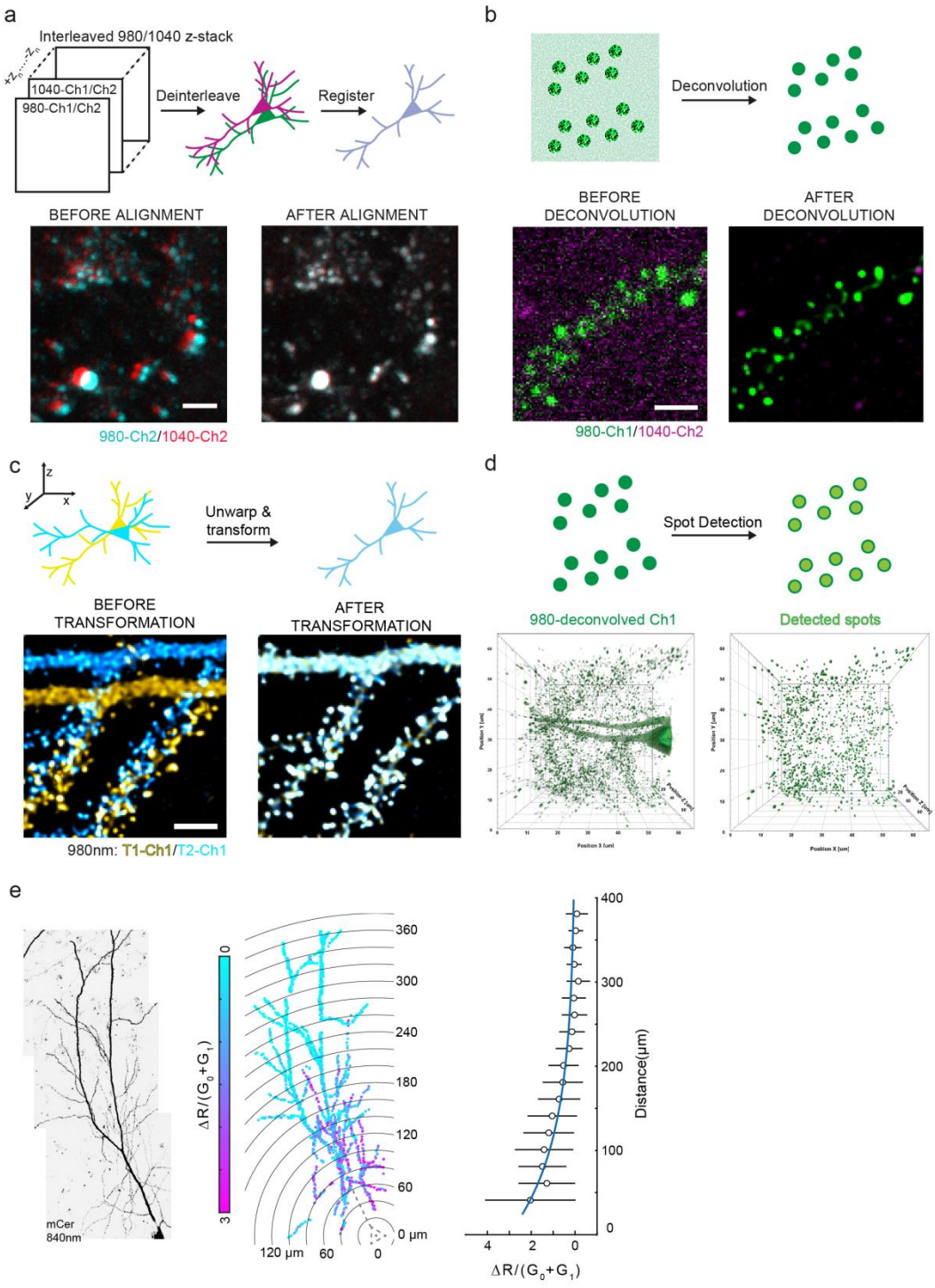

Figure 5 | Analysis workflow for automated detection and analysis of SynTagMA photoconversion.

(a) The green and red channels of interleaved z-stacks taken from neurons expressing postSynTagMA (two-photon excitation 980 nm and 1040 nm) are registered to correct for chromatic aberration. Scale bar 4 µm. **(b)** Median filtering and deconvolution is then applied to all images in both green and red channels. Scale bar 3 µm. **(c)** Using the green channels, unwarping and transformation is applied to successive z-stacks to account for local changes in 3D position due to tissue distortion and spine movement. Scale bar 4 µm. **(d)** Synapses (ROIs) are detected as spherical objects. **(e)** Maximum intensity projection of a CA1 pyramidal cell expressing cytosolic mCerulean (inverted gray scale) and postSynTagMA (left). $\Delta R/(G_0 + G_1)$ for each identified synapse at its location in the projected image (photoconversion with 50 bAPs (100 Hz) as in Fig. 4). Dashed line indicates primary first-order apical dendrite, which was not analyzed, and soma position. At right is plotted the median and interquartile range binned in concentric rings (20 µm width) radiating from the soma. Photoconversion decreased exponentially from the soma with a length constant of λ = 105 µm (n = 1860 synapses, R^2 = 0.914).

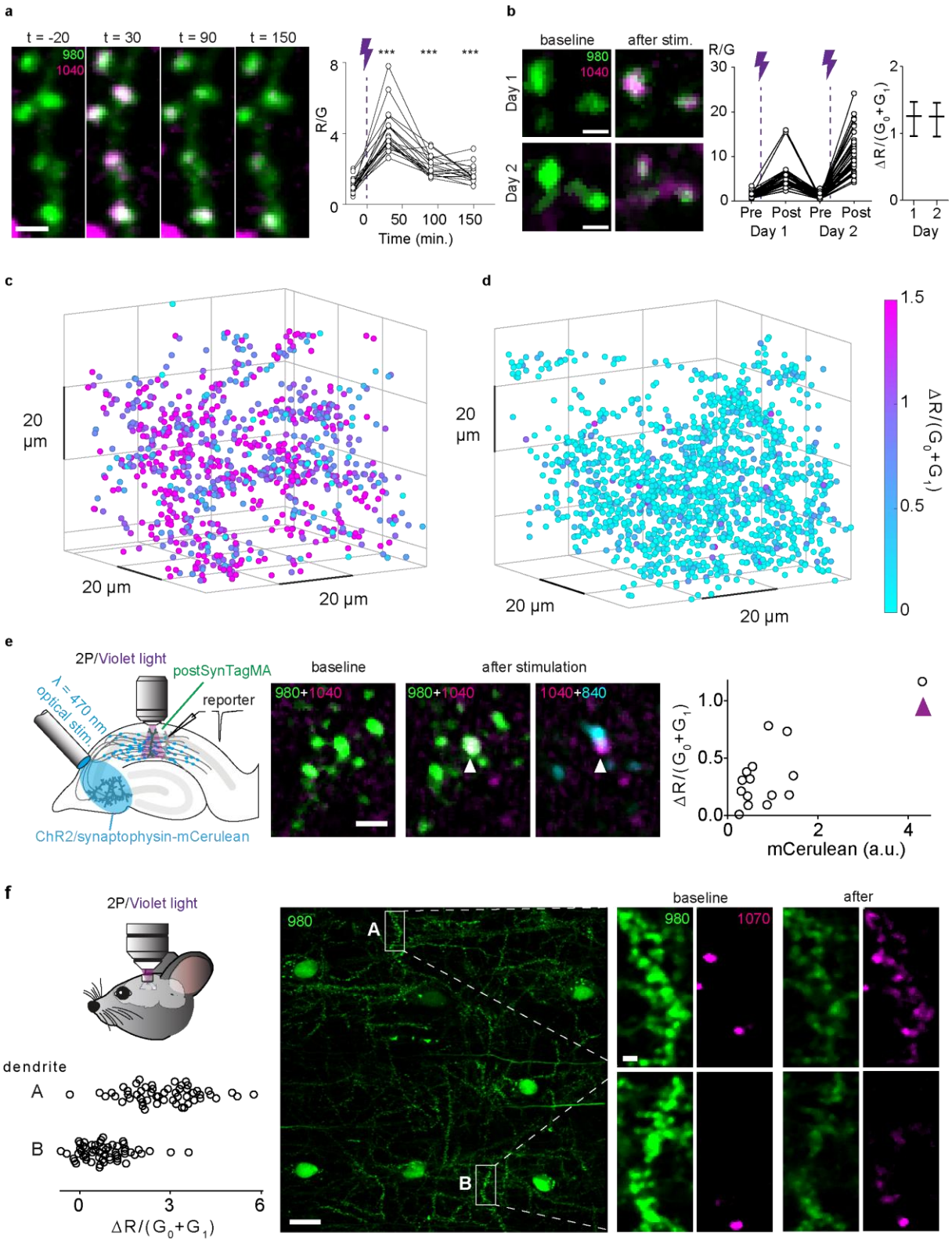

Figure 6 | Using postSynTagMA to study synaptic activity.

(a) Ratio images and summary plot of spines from a CA1 pyramidal neuron expressing postSynTagMA and mCerulean taken before (-20 min.) and after (30 min., 90 min., 150 min.) photoconverting (395 nm, 16 mW mm^{-}

^{2}, 2 s, t = 0 min.) while stimulating presynaptic axons in *stratum radiatum* (100 x at 100 Hz). τ = 57 min, n = 19 synapses, ***p < 0.0001, Friedman nonparametric test for repeated measures). Scale bar 2 µm. **(b)** Ratio images before and after photoconversion of the same stretch of dendrite on successive days (left, 18 hours between). Suprathreshold extracellular synaptic stimulation was paired with violet light pulses (500 ms, 1s delay, 15x) to photoconvert postSynTagMA. Plotted are R/G of each of n = 37 synapses and median $\Delta R/(G_0 + G_1)$ and inter-quartile range for each day. Scale bar 1 µm. **(c)** Color-coded $\Delta R/(G_0 + G_1)$ of spines plotted at their location in the 60 x 60 µm volume of tissue imaged. Suprathreshold stimulation of synaptic inputs in *stratum radiatum* was paired with violet light as in b). Note that $\Delta R/(G_0 + G_1)$ is equal or greater than 1.5 (magenta) for most of the spines (n = 897 synapses). **(d)** As in c) but the extracellular stimulation was subthreshold. Note that $\Delta R/(G_0+G_1)$ is greater than 1 (magenta) for only a few scattered synapses (n = 1502). **(e)** CA3 neurons expressing ChR2-ET/TC and synaptophysin-mCerulean were stimulated with 470 nm flashes to evoke subthreshold (~500 pA) synaptic responses in a neighboring neuron (50 repeats) while flashing violet light (50 repeats, 100 ms, 395 nm, 16 mW mm^{-2}) through the objective onto a postSyntagMA expressing CA1 neuron. Images are overlays of green/red SynTagMA fluorescence (green/magenta) or SynTagMA red/mCerulean (magenta/cyan). Note the apposition of a synaptophysin-mCerulean bouton to a photoconverted synapse (white arrows, magenta arrow in plot). Scale bar 2 µm. **(f)** *In vivo* 2P imaging of AAV9-mDlx-postSynTagMA expressing interneurons in mouse hippocampus through a chronic cranial window (left). Widefield image of interneurons in *stratum oriens* and close-up of dendrites A and B, indicated by the white boxes. Green and red fluorescence was excited at 980 nm and 1070 nm, respectively. Violet light (20 flashes, 0.2 Hz, 3 s duration, 0.42 mW mm^{-2}) was applied to photoconvert postSynTagMA. Plotted at left are the photoconversion ratios from dendrite A (n = 54 synapses) and B (n = 58 synapses). Scale bars: wide field 20 µm, dendrites 2 µm.

Material & Methods

Plasmids

To create preSynTagMA (available from Addgene # 119738), synaptophysin-GCaMP3 (kindly provided by Loren Looger, Janelia Farms, HHMI) was, as previously described[1], digested by HindIII and BamHI to remove GCaMP3, and CaMPARI was fused to synaptophysin using the In-Fusion® HD Cloning method and kit (Takara Bio USA) after amplifying variants of CaMPARI with PCR using custom primers with base pair overhangs homologous to the synaptophysin plasmid (3' Primer [CGATAAGCTTTTATGAGCTCAGCCGACC], 5' Primer [CAGATGAAGCTTATGCTGCAGAACGAGCTTG]).

To create postSynTagMA (available on Addgene # 119736) and other related constructs, we followed several steps. After removal of restriction site XbaI from pCAG_PSD95.FingR-eGFP-CCR5TC (a gift from Don Arnold, Addgene # 46295), PSD95.FingR-eGFP-CCR5TC was inserted into a pAAV-hsyn1 backbone (Addgene # 101361) without the CAG promoter or upstream zinc finger binding site, to produce pAAV-syn-PSD95.FingR-eGFP-CCR5TC (available upon request). The eGFP was then replaced with CaMPARI1[2] (Addgene # 60421), from which we had deleted the nuclear export signal (NES), to produce pAAV-syn-PSD95.FingR-dNES-CaMPARI1-CCR5TC, a fusion construct of the fibronectin intrabody and a CaMPARI variant that is not restricted to the cytosol and can enter the nucleus. To finally generate pAAV-syn-postSynTagMA, CaMPARI1 was then replaced by CaMPARI2 (without NES and epitope tags) and the point mutations F391W and L398V were introduced using QuickChange PCR to increase calcium affinity[3]. The left-handed zinc finger (aka CCR5TC) fused to the KRAB(A) transcriptional repressor[4] was removed to produce pAAV-syn-PSD95.FingR-dNES-CaMPARI2_F391W_L398V, the unregulated variant. A sequence including the zinc finger binding sequence (5'-GTCATCCTCATC-3')[5,6] upstream of the hsyn1 promoter was synthesized (ThermoFisher) and inserted using the MluI and EcoRI restriction sites to generate pAAV-ZFBS-syn-PSD95.FingR-dNES-CaMPARI2_F391W_L398V-CCR5TC. Other plasmids such as the lower affinity pAAV-syn-PSD95.FingR-dNES-CaMPARI2-CCR5TC, pAAV-syn-synaptophysin-CaMPARI2 and the variants with zinc finger binding sequence are available upon request. The cytosolic CaMPARI2 variant pAAV-hsyn-NES-his-CaMPARI2-F391W-L398V[3] is also available from Addgene # 119723. mCerulean was kindly provided by Dr. Wolfang Wagner (ZMNH) and cloned into a pCI-syn backbone.

Animals

All animal experiments were performed according to local law and were approved by the local authorities. In Hamburg, Germany, Wistar rats and C57BL/6 mice were housed and bred at the University Medical Center Hamburg-Eppendorf. All procedures were performed in compliance with German law according and the guidelines of Directive 2010/63/EU. Protocols were approved by the Behörde für Gesundheit und Verbraucherschutz of the City of Hamburg. In New Hampshire, USA, experiments with Sprague-Dawley rats were approved by Dartmouth College's Institutional Animal Care and Use Committee (IACUC).

Dissociated neuron cell culture

Neurons from P1 Sprague-Dawley rats of either sex were isolated from hippocampal CA1-CA3 regions with dentate gyrus removed, dissociated (bovine pancreas trypsin; 5 min at room temperature), and plated on polyornithine-coated coverslips inside a 6 mm diameter cloning cylinder. Calcium phosphate-mediated gene transfer was used to transfect 5-7 day old cultures. All measurements unless otherwise noted, are from mature 13-21 day old neurons.

Cell culture imaging

SypCaMPARI experiments (Figure 1) were performed at 34˚ C using a custom-built objective heater. Coverslips were mounted in a rapid-switching, laminar-flow perfusion and stimulation chamber on the stage of a custom-built laser microscope. The volume of the chamber was maintained at ~75 µl and was perfused at a rate of 400 µl/min. Neurons were perfused continuously during imaging with a standard saline solution containing the following in mM: 119 NaCl, 2.5 KCl, 2$CaCl_2$, 2$MgCl_2$, 25 HEPES, 30 D-Glucose, 10 µM 6-cyano-7-nitroquinoxaline-2,3-dione (Sigma), and 50 µM D,L-2-amino-5-phosphovaleric acid (Sigma). Tetrodotoxin (TTX; Alomone Labs) was used at a final concentration of 3 µM in standard saline solution during perfusion when noted. Bicuculline (Tocris) was used at a final concentration of 20 µM.

Syp-CaMPARI green fluorescence was measured by illuminating neurons with a 488 nm laser (Coherent OBIS laser, ~ 3 mW) with a ZET488/10x and ZT488rdc dichroic (Chroma). Red fluorescence was measured by illuminating neurons with a 561 nm laser (Coherent OBIS laser) with ZET561/10x and ZT561rdc dichroic (Chroma). All channels were imaged through either a Zeiss EC Plan-Neofluar 40x 1.3 NA objective or an Olympus UAPON40XO340-2 40x 1.35 NA objective. Emission in the green spectra was collected using an ET 525/50m filter (Chroma) and emission in the red spectra was collected using an ET600/50m filter (Chroma). All emission light was collected using an IXON Ultra 897 EMCCD camera (Andor). SypCaMPARI fluorescence was collected with an exposure time of 39.72 ms and images were acquired at 25 Hz.

Cell culture stimulation and photoconversion

Field stimulation-evoked action potentials were generated by passing 1 ms current pulses, yielding fields of ~12 Vcm^2 through the recording chamber bracketed by Platinum/Iridium electrodes. Electrical stimuli were locked to start according to defined frame number intervals using a custom-built board named “Neurosync” powered by an Arduino Duo chip (Arduino) manufactured by an engineering firm (Sensostar)[7]. A collimated 405 nm LED light source (Thorlabs) was set on top of the microscope stage with a custom-built plastic case (Bob Robertson, Dartmouth College). This light source was coupled to a T-Cube LED Driver (Thorlabs) and a Pulse Pal (Open Ephys) was used to trigger light flashes of specific duration and delay. The light source trigger was set relative to a TTL input from Neurosync. Power density of the 405 nm light was measured using a digital handheld optical power and energy meter console with an attached photodiode power sensor (Thorlabs). The power densities used were either 10.8 mW cm^{-2} or 54.1 mW cm^{-2}.

For incubator photoconversion experiments (Supplementary Fig. 2), custom-built circular 51-diode 405 nm LED arrays (Ultrafire) were wired up to a custom dual programmable relay board to flash light for 100 ms every 10 s, inside a cell culture incubator (New Brunswick; Eppendorf) set to ~37˚ C and ~5% CO_2. Neurons were then mounted on the microscope with perfusion, and green fluorescence was imaged during 50 stimulations @ 50Hz

(as above) to measure calcium-dependent dimming. Only neurons responsive to stimulation were then analyzed (over ~90% of cells measured).

Patterned time-locking photoconversion

Time locking experiments (Fig. 2, Supplementary Fig. 1) were performed on a Nikon Ti-E microscope fitted with an Andor W1 Dual Camera (Andor CMOS ZYLA), dual spinning disk, Coherent Lasers (OBIS 405, 488 and 561 nm) and the Andor Mosaic 3 micromirror mosaic system, controlled by Andor iQ software, and Nikon elements for image acquisition. A Pulse Pal was used to time lock the stimulus with the mosaic sequence start. A custom 5x5, 250 μm^2 square grid was drawn within the illuminated mosaic field and counterbalanced the different time sequences across various regions of the field.

Neuron culture image analysis

EMCCD camera images or confocal image stacks were imported into Fiji. A maximum intensity projection was made from the confocal stacks. Ten pixel diameter circular ROIs were placed over boutons identified by eye using a custom written plugin to localize them over the brightest pixel in the green channel (https://imagej.nih.gov/ij/plugins/time-series.html). Boutons were identified as punctate spots that showed a dimming response to AP stimulation (>98% of punctate spots). ROIs were centered on the brightest green pixel in the green channel and average intensity was measured for red and green channels. Average background fluorescence was determined from several larger ROIs placed across the imaging field where there were no transfected axons. The average green and red background fluorescence was subtracted from the respective values before calculating ratios or $\Delta F/F$.

Rat hippocampal slice cultures

Hippocampal slice cultures from Wistar rats were prepared at postnatal day 4–7 as described[8]. No antibiotics were present in the culture medium. At DIV 13-17, neurons were transfected by single-cell electroporation[9]. Thin-walled pipettes (~10 MΩ) were filled with intracellular K-gluconate based solution into which SynTagMA plasmid DNA was diluted to 20 ng μl^{-1}. In some experiments, a plasmid expressing mCerulean was also included in the pipette at 20 ng μl^{-1}. The intracellular solution contained in (mM): 135 K-gluconate, 4 $MgCl_2$, 4 Na_2-ATP, 0.4 Na-GTP, 10 Na_2-phosphocreatine, 3 ascorbate, 0.02 Alexa Fluor 594, and 10 HEPES (pH 7.2). Pipettes were positioned against neurons and DNA was ejected using an Axoporator 800A (Molecular Devices) with 50 hyperpolarizing pulses (-12 V, 0.5 ms) at 50 Hz.

Two-Photon microscopy in hippocampal slice cultures

Experiments were performed 3-4 days after electroporation (DIV 16-20). The custom-built two-photon imaging setup was based on an Olympus BX51WI microscope equipped with a LUMPlan W-IR2 60× 0.9 NA (Olympus) or a W Plan-Apochromat 40× 1.0NA (Zeiss) objective, controlled by the open-source software package ScanImage[10]. Two pulsed Ti:Sapphire lasers (MaiTai DeepSee, Spectra Physics) controlled by electro-optic modulators (350-80, Conoptics) were used to excite SynTagMA green (980 nm) and red species (1040 nm), respectively. Z-stacks of SynTagMA-expressing neurons were acquired above Nyquist rate. Each plane was scanned twice, using first 980 nm excitation (green fluorescence) and then 1040 nm excitation (red fluorescence) before moving to the next plane. For quantification of pre or postsynaptic targeting, axons of CA3 cells or oblique dendrites of CA1 neurons

expressing mCerulean and pre- or postSynTagMA, respectively, were imaged in *stratum radiatum* at 840 nm and 980 nm, respectively. Separate stacks were taken using excitation at 840 nm to image mCerulean when both 980 nm and 1040 nm were being used to image SynTagMA. Emitted photons were collected through the objective and oil-immersion condenser (1.4 NA, Olympus) with two pairs of photomultiplier tubes (H7422P-40, Hamamatsu). 560 DXCR dichroic mirrors and 525/50 and 607/70 emission filters (Chroma Technology) were used to separate green and red fluorescence. Excitation light was blocked by short-pass filters (ET700SP-2P, Chroma). Two brief violet light pulses (395 nm, 100 ms, 16 mW mm^{-2}, 0.1 Hz) were delivered through the objective using a Spectra X Light Engine (Lumencor) just before imaging to photoswitch the CaMPARI moiety into its bright state[2].

Electrophysiology

Hippocampal slice cultures were placed in the recording chamber of the two-photon laser scanning microscope and continuously perfused with an artificial cerebrospinal fluid saturated with 95% O_2 and 5% CO_2 consisting of (in mM): 119 NaCl, 26.2 $NaHCO_3$, 11 D-glucose, 1 NaH_2PO_4, 2.5 KCl, 4 $CaCl_2$, 4 $MgCl_2$. (pH 7.4, 308 mOsm) at room temperature (21-23 °C) or with a HEPES-buffered solution (in mM): 135 NaCl, 2.5 KCl, 10 Na-HEPES, 12.5 D-glucose, 1.25 NaH_2PO_4, 4 $CaCl_2$, 4 $MgCl_2$ (pH 7.4). Whole-cell recordings from CA1 pyramidal neurons were made with patch pipettes (3–4 MΩ) filled with (in mM): 135 K-gluconate, 4 $MgCl_2$, 4 Na_2-ATP, 0.4 Na-GTP, 10 Na_2-phosphocreatine, 3 ascorbate, and 10 HEPES (pH 7.2, 295 mOsm). Series resistance was below 20 MΩ. A Multiclamp 700B amplifier (Molecular Devices) was used under the control of Ephus[11] software written in Matlab (The MathWorks). When using somatic current injection to evoke action potentials in SynTagMA expressing neurons, the antagonists CPPene (10 µM) and NBQX (10 µM) (both from Tocris) were added to the extracellular recording solution to block synaptic transmission. For extracellular synaptic stimulation, a monopolar electrode was placed in *stratum radiatum* and two 0.2 ms pulses, 40 ms apart, were delivered using an ISO-Flex stimulator (A.M.P.I.). Stimulation intensity was adjusted to be subthreshold for action potentials (i.e. to evoke ~15 mV EPSPs or ~-500 pA EPSCs) or suprathreshold (i.e. evoking action potentials) by patching a nearby neuron in CA1. To optically stimulate ChR2-expressing CA3 neurons we used a micromanipulator to position the end of a fiber-optic cable to illuminate the CA3 neurons with blue light.

Photoconversion in hippocampal slice cultures

Photoconversion was achieved by delivery of violet light (duration 100 ms – 2 s as indicated in figure legends, 395 nm, 16 mW mm^{-2}) using a Spectra X Light Engine (Lumencor) coupled with an optical fiber to the epifluorescence port of the two-photon microscope. During the violet light pulses, shutters (Uniblitz) protected the photomultiplier tubes. We typically used 100-500 ms violet light pulses repeated 15-50 times with a 1 s delay from stimulus onset to photoconvert postSynTagMA. An image stack was always taken prior to and following photoconversion. In the bAP experiments, we acquired the first image stack before patching the SynTagMA neuron. The cell was then whole-cell patch-clamped and bAPs (100 Hz) were evoked by somatic current injection and paired with photoconversion light. While acquiring the second image stack, the cell was held in voltage clamp at -65 mV to prevent further action potentials. To monitor turnover of photoconverted SynTagMA, a monopolar glass electrode filled with ACSF was placed in *stratum radiatum* to strongly stimulate synapses onto CA1 postSynTagMA-expressing neurons (100 pulses of 0.2 ms duration, at 100 Hz). Stimulation intensity was adjusted to induce spiking in a neighboring post-synaptic cell. Photoconversion was achieved by

delivery of violet light (395 nm, 2 s, 16 mW mm^{-2}) with a 1 s delay from stimulus onset. For relabeling experiments, paired-pulse electrical stimulation (0.2 ms pulses, 40 ms apart) was combined with 250 ms of violet light. This was repeated 25 times at 5 s intervals and a second image stack was acquired immediately thereafter. After imaging, slices were returned to the incubator. About 18 hrs later, the same procedure was repeated.

Optogenetic stimulation

An AAV2/9 synapsin-ChR(ET/TC)-2A-synaptophysin-mCerulean, prepared by Dr. Ingke Braren at the UKE vector facility was injected locally into CA3 of slice cultures at DIV 7. Additionally, several CA1 neurons were electroporated with postSynTagMA (20 ng μl^{-1}) at DIV 22. After allowing 3 days for expression, CA3 neurons were stimulated with blue light pulses (470 nm, 2 pulses, 2-5 ms duration, 40 ms apart) applied through a light fiber positioned under the objective pointed towards CA3. The light intensity and pulse width were set to evoke EPSCs (0.5 – 1.0 nA) in a CA1 neuron close to the postSynTagMA expressing neurons. Pairing stimulation with violet light (1 s delay, 395 nm, 100 ms, 16 mW mm^{-2}) was repeated 50 times at 0.1 Hz to photoconvert postSynTagMA in active spines. Green/red interleaved z-stacks of spiny dendrites were acquired before and after photoconversion. The third z-stack to image the mCerulean labelled boutons was acquired immediately after the post-photoconversion stack.

3D image analysis with manual ROI selection

A macro written in Fiji[12] was used for two-photon 3D image analysis at 840, 980 and/or 1040 nm wavelengths. When z-stacks contained alternating images collected at 2 excitation wavelengths, they were first separated and then xyz-aligned to correct for chromatic aberration using green and/or red channels and the pairwise stitching plugin[13]. mCerulean and SynTagMA fluorescence values were obtained from images after median filtering and rolling ball background subtraction[14]. Regions of interest (ROI) were drawn onto maximum intensity projections and compared to axonal or dendrite shafts, respectively. Only spines projecting laterally from the dendrite were analyzed.

For the initial characterization of postSynTagMA, quantification of green to red conversion was performed manually in a small sets of synapses (<50) in Matlab and/or Fiji. Covering relative larger areas of the dendritic tree gave rise to larger data sets (>1000 synapses) that made a semi-automated analysis approach necessary. After rigid registration performed using the Pairwise stitching plugin[13] in Fiji, 2P images were further processed using a blind deconvolution algorithm in Autoquant X3 (MediaCybernetics). Particularly critical was to correct for position change of synapses in 3D due to tissue deformation (“warping”) between acquisitions of images, i.e. pre- and post- violet light application. To correct for tissue warping, synapse voxels were reassigned to their initial position using either elastix[15] or ANTs (Advanced Normalization Tools)[16]. Synapse detection in 2P z-stacks was performed using the Imaris 3D spot detection feature (Bitplane AG) using the G_0 deconvolved signal. Imaris ‘Spots’ are then used as volumetric ROIs to extract fluorescence values from green and red channels (maximum pixel values from raw images, median filtered) at every time point. Green (G_0 and G_1) and red (R_0 and R_1) values used for metric calculation were normalized dividing by the mean value of G_0 and R_0, respectively.

Automated segmentation and analysis of SynTagMA data

To analyze thousands of synapses in large 3D datasets using a single program, we developed a pipeline to automatically identify spots in 3D and define volumes (ROIs) for accurate measurements of fluorescence changes (see flow chart below). All steps of our workflow are controlled through a GUI written in Matlab, named SynapseLocator, which calls specific subroutines (Fiji, elastix, Weka). A specific challenge is posed by local movements of individual synapses between time points of data acquisition, which makes *post hoc* alignment and de-warping of images a lengthy but essential step prior to segmentation. A typical experiment consists of at least two time points (before / after stimulation) in which green and red fluorescence is collected simultaneously alternating between 980 and 1040 nm excitation at every optical section of the z-stack. For each time point, we correct channel misalignment due to chromatic aberration by performing rigid registration of the de-interleaved two-color images in Matlab. The detailed workflow in SynapseLocator consists of an initial deconvolution step (Fiji, DeconvolutionLab2[17] plugin) in which diffraction-induced blurring of the images is reduced. Input image stacks (only green channel; G_0 and G_1) are then loaded and prepared for running an image registration with elastix[15]. The registration is comprised of four steps (rigid transformation, rotation transformation, affine transformation, and non-rigid registration) for which the optimized parameter sets are suggested. The transformation is then applied to both red and green channel data (deconvolved and raw). Synapse detection involves a machine learning process accessed via Fiji (Weka, Trainable Weka Segmentation plugin).[18] Two classes are manually identified ("spot", "no spot"), by a user, to train a random forest model considering a set of scale-invariant image features (Hessian and Laplacian, each calculated at three scales, Fiji, FeatureJ plugin). A synapse is identified as a region in which a group of voxels with spot class properties shows minimal connectivity (26-connected neighborhood). For each region, an ellipsoid enclosing the identified connected voxels is calculated in Matlab and stored as ROI. Regions are further filtered by size to exclude objects with extreme measures. Inclusion criteria for synapses are: green initial signal (G_0) above background, red initial signal (R_0) below red background, and shape correlation values between G_0 and R_1. Converted synapses are identified according to their "conversion-factor" ($\Delta R/(G_0+ G_1)$). We have deposited SynapseLocator at GitHub (https://github.com/drchrisch/SynapseLocator) together with instructions and example data.

Image processing flow chart

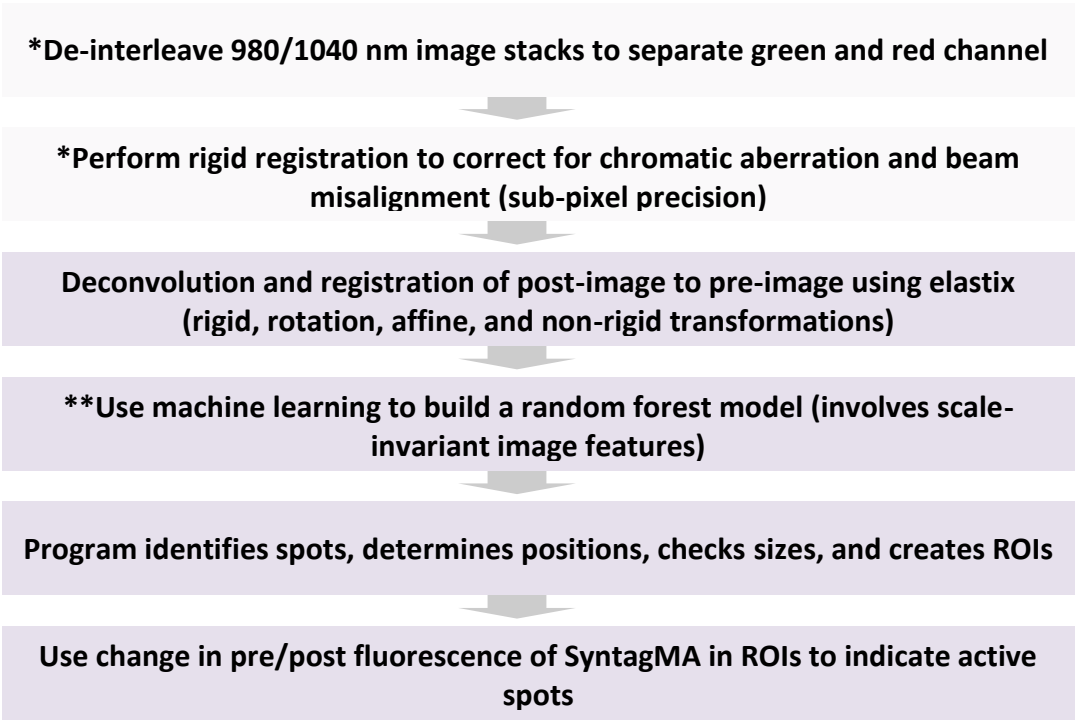

*Pre-processing steps (microscope-specific), prior to loading into SynapseLocator
** Typically, the model is robust enough to allow for analysis of all experiments from a series.

Distance-dependence of back-propogating action potentials

CA1 neurons expressing mCerulean and postSynTagMA were used for these experiments. Prior to patching the neurons, 2 series of z-stacks were acquired along the apical dendritic tree, one at 840 nm (mCerulean) and one interleaving 980nm and 1040nm. Each 1024 x 1024 pixel z-stack covered a 150 µm x 150 µm area with depths varying between 50-100 microns. Two to three stacks were required to image the apical dendritic tree. The time taken to image all stacks was 30-40 minutes. After acquiring the first series of images, the cell was whole-cell patch-clamped and 50 bAPs paired with 500ms violet light (395 nm, 16 mW mm^{-2}, 1 s delay) was repeated 15 times. Immediately after, all red/green image stacks were acquired.

Virus injection and hippocampal window surgery for in vivo experiments

Male, adult C57BL/6 mice injected with an AAV2/9 encoding mDlx-SynTagMA-2A-mCerulean were used for in vivo imaging experiments at the age of 4-5 months. The mice were housed in pathogen-free conditions, the light/dark cycle was 12/12 h and the humidity and temperature were kept constant (40% relative humidity; 22°C). Mice were anesthetized with an intraperitoneal injection of ketamine/xylazine (0.13/0.01 mg/g bodyweight) and placed on a heating blanket to maintain the body temperature. In addition, mice received a subcutaneous dose of Carprofen (4 mg/kg) for post-surgery analgesia. Eyes were covered with eye ointment (Vidisic, Bausch + Lomb) to prevent drying. Prior to surgery, the depth of anesthesia and analgesia was evaluated with a toe-pinch to test the paw-withdrawal reflex. Subsequently, mice were fixed in a stereotactic frame, the fur was removed with a fine trimmer and the skin of the head was disinfected with Betaisodona solution using

sterile cotton swabs. The skin was removed by a midline scalp incision (1-3 cm), the skull was cleaned using a bone scraper (Fine Science Tools) and a small hole was drilled with a dental drill (Foredom) above the injection site. Injection of an AAV2/9 viral vector carrying the mDlx-SynTagMA-2A-mCerulean cDNA was targeted unilaterally to the dorsal CA1 area (− 2.0 mm anteroposterior (AP), ± 1.3 mm mediolateral (ML), − 1.6 mm dorsoventral (DV) relative to Bregma). 0.6 µl of virus suspension was injected at 100 nl/min using a glass micropipette. After the injection, the needle stayed in place for at least 5 min after virus delivery before it was withdrawn and the scalp was closed with sutures. During the two days following surgery animals were provided with Meloxicam mixed into soft food.

2 weeks after virus injection, the mice were anesthetized by the same procedure as described above to implant the hippocampal window. After fur removal, skin above the frontal and parietal bones of the skull was removed by one horizontal cut along basis of skull and two rostral cuts. The skull was cleaned after removal of the periosteum, roughened with a bone scraper and covered with a thin layer of cyanoacrylate glue (Cyano Veneer). After polymerization a 3-mm circle was marked on the right parietal bone (anteroposterior, −2.2 mm; mediolateral, +1.8 mm relative to bregma) with a biopsy punch and the bone was removed with a dental drill (Foredom). The bone fragment and dura were carefully removed with fine surgical forceps. The cortex above the hippocampus was aspirated with a 0.8 mm blunt needle connected to a water jet pump. When first layer of fibers running orthogonal to midline became visible, a 0.4 mm blunt needle was used to carefully remove the upper two of three fiber layers of the external capsule. Absorbable gelatin sponges (Gelfoam, Pfizer) were used to control bleeding. The craniotomy was washed with sterile PBS and a custom-built imaging window was inserted over the dorsal hippocampus. The window consisted of a hollow glass cylinder (diam.: 3 mm, wall thickness: 0.1 mm, height: 1.5 mm) glued to a No. 1 coverslip (diam.: 3mm, thickness: 0.17 mm) on the bottom and to a stainless steel rim on the top with UV-curable glass glue (Norland NOA61). The steel rim and a head holder plate (Luigs & Neumann) were fixed to the skull with cyanoacrylate gel (Pattex). After polymerization, cranial window and head holder plate were covered with dental cement (Super Bond C&B, Sun Medical) to provide strong bonding to the skull bone. During the two days following surgery animals were provided with Meloxicam mixed into soft food.

Hippocampal imaging and photoconversion *in vivo*

Mice were anesthetized with isoflurane at a concentration ranging between 2.0% and 2.5% in 100% O_2, fixed under the microscope at the head holder plate (Luigs & Neumann) and placed on a heating blanket to maintain the body temperature. Eyes were covered with eye ointment (Vidisic, Bausch + Lomb) to prevent drying. The window was centered under the two-photon microscope (MOM-scope, Sutter Instruments, modified by Rapp Optoelectronics) using a low-magnification objective (4x Nikon Plan Fluorite) and SynTagMA-expression was verified in the hippocampus using epi fluorescence. The cranial window was then filled with water to image SynTagMA in two-photon mode through a 40x objective (40X Nikon CFI APO NIR, 0.80 NA, 3.5 mm WD). The green species of SynTagMA was excited with a Ti:Sa laser (Chameleon Vision-S, Coherent) tuned to 980 nm. The red species of SynTagMA was excited with an ytterbium-doped 1070-nm fiber laser (Fidelity-2, Coherent). Single planes (512x512 pixels) were acquired at 30 Hz with a resonant-galvanometric scanner at 29-60 mW (980 nm) and 41-60 mW (1070 nm) using ScanImage 2017b (Vidrio). Emitted photons were detected by a pair of photomultiplier tubes (H7422P-40, Hamamatsu). A 560 DXCR dichroic mirror and 525/50 and 607/70 emission

filters (Chroma Technology) were used to separate green and red fluorescence. Excitation light was blocked by short-pass filters (ET700SP-2P, Chroma). Since SynTagMA fluorescence was relatively low, 450 – 1800 frames per optical plane were acquired and averaged. The conversion protocol consisted of 3 s violet light pulses (385 nm, 0.42 mW mm^{-2}) repeated 20 times through the imaging objective at a 5 s time interval. Motion artefacts were corrected with a custom-modified Lucas-Kanade-based alignment algorithm in Matlab.

Statistics

All statistics were performed using GraphPad Prism (v8) or Matlab. For data with normal distributions, Student's t-test or one-way ANOVA were used. Data considered non-normal (according to a D'Agostino-Pearson test) underwent non-parametric tests (Kruskal-Wallis). For detailed information on statistical tests done in each figure, see figure legends and supplementary table 1.

References

1. Hoppa, M. B., Lana, B., Margas, W., Dolphin, A. C. & Ryan, T. A. α2δ expression sets presynaptic calcium channel abundance and release probability. *Nature* **486,** 122–125 (2012).
2. Fosque, B. F. *et al.* Labeling of active neural circuits in vivo with designed calcium integrators. *Science* **347,** 755–760 (2015).
3. Moeyaert, B. *et al.* Improved methods for marking active neuron populations. *Nature communications* **9,** 4440 (2018).
4. Margolin, J. F. *et al.* Krüppel-associated boxes are potent transcriptional repression domains. *Proceedings of the National Academy of Sciences of the United States of America* **91,** 4509–13 (1994).
5. Perez, E. E. *et al.* Establishment of HIV-1 resistance in CD4+ T cells by genome editing using zinc-finger nucleases. *Nature Biotechnology* **26,** 808–816 (2008).
6. Gross, G. G. *et al.* Recombinant probes for visualizing endogenous synaptic proteins in living neurons. *Neuron* **78,** 971–85 (2013).
7. Cho, I. H., Panzera, L. C., Chin, M. & Hoppa, M. B. Sodium Channel β2 Subunits Prevent Action Potential Propagation Failures at Axonal Branch Points. *The Journal of neuroscience : the official journal of the Society for Neuroscience* **37,** 9519–9533 (2017).
8. Gee, C. E., Ohmert, I., Wiegert, J. S. & Oertner, T. G. Preparation of Slice Cultures from Rodent Hippocampus. *Cold Spring Harbor Protocols* **2017,** pdb.prot094888 (2017).
9. Wiegert, J. S., Gee, C. E. & Oertner, T. G. Single-Cell Electroporation of Neurons. *Cold Spring Harbor Protocols* **2017,** pdb.prot094904 (2017).
10. Pologruto, T. a, Sabatini, B. L. & Svoboda, K. ScanImage: flexible software for operating laser scanning microscopes. *Biomedical engineering online* **2,** 13 (2003).
11. Suter, B. A. *et al.* Ephus: multipurpose data acquisition software for neuroscience experiments. *Frontiers in neural circuits* **4,** 100 (2010).
12. Schindelin, J. *et al.* Fiji: an open-source platform for biological-image analysis. *Nature Methods* **9,** 676–682 (2012).
13. Preibisch, S., Saalfeld, S. & Tomancak, P. Globally optimal stitching of tiled 3D microscopic image acquisitions. *Bioinformatics (Oxford, England)* **25,** 1463–5 (2009).
14. Sternberg. Biomedical Image Processing. *Computer* **16,** 22–34 (1983).
15. Klein, S., Staring, M., Murphy, K., Viergever, M. A. & Pluim, J. elastix: A Toolbox for Intensity-Based Medical Image Registration. *IEEE Transactions on Medical Imaging* **29,** 196–205 (2010).
16. Avants, B. B. *et al.* A reproducible evaluation of ANTs similarity metric performance in brain image registration. *NeuroImage* **54,** 2033–44 (2011).
17. Sage, D. *et al.* DeconvolutionLab2: An open-source software for deconvolution microscopy. *Methods* **115,** 28–41 (2017).
18. Arganda-Carreras, I. *et al.* Trainable Weka Segmentation: a machine learning tool for microscopy pixel classification. *Bioinformatics (Oxford, England)* **33,** 2424–2426 (2017).